

Elastic Bag Model for Molecular Dynamics Simulations of Solvated Systems: Application to Liquid Argon

Yuhui Li, Goran Krilov, and B. J. Berne*

Department of Chemistry, Columbia University, 3000 Broadway, New York, New York 10027

Received: July 15, 2004; In Final Form: October 19, 2004

A new approach is developed to study the dynamics of the localized process in solutions and other condensed phase systems. The approach employs a fluctuating elastic boundary (FEB) model which encloses the simulated system in an elastic bag that mimics the effects of the bulk solvent. This alleviates the need for periodic boundary conditions and allows for a reduction in the number of solvent molecules that need to be included in the simulation. The boundary bag is modeled as a mesh of quasi-particles connected by elastic bonds. The FEB model allows for volume and density fluctuations characteristic of the bulk system, and the shape of the boundary fluctuates during the course of the simulation to adapt to the configuration fluctuations of the explicit solute–solvent system inside. The method is applied to the simulation of a Lennard-Jones model of liquid argon. Various structural and dynamical quantities are computed and compared with those obtained from conventional periodic boundary simulations. The agreement between the two is excellent in most cases, thus validating the viability of the FEB method.

I. Introduction

Molecular dynamics (MD) simulations have provided a basis for understanding the structure and dynamics of protein molecules. The choice of boundary conditions plays an important role in molecular dynamics simulations of condensed phase systems. Periodic boundary conditions are conventionally used to accurately model the bulk solution by only 10^2 – 10^4 particles.¹ On the other hand, many reactive processes of interest in liquids are characterized by spatial localization. For example, an enzyme-catalyzed reaction occurs in a spatially well-defined active site of the protein. To study such processes, we are interested in the trajectory of a relatively few atoms. However, under the traditional periodic boundary approach, a significant amount of computational time is consumed in computing the trajectories of solvent molecules, large numbers of which must be included to accurately model the environment of the solvated reaction center. As a result, the use of molecular dynamics with periodic boundary conditions is inefficient. Another case where the direct use of periodic boundary conditions is not suitable includes the study of inhomogeneous systems and nonequilibrium phenomena. For instance, the use of periodic boundary conditions to model a nonequilibrium system with a thermal gradient is inappropriate.

Numerous methods have been developed in an attempt to reduce the computational time and avoid the difficulties associated with periodic boundary conditions. The MTGLE method, developed by Berkowitz, Brooks, and Adelman,^{2–4} represents one of the first approaches to modeling the localized processes in the condensed phase based on partitioning the system into a primary part, consisting of a few relevant degrees of freedom, and a secondary part which consists of the remaining degrees of freedom and functions as a heat bath for the first. In the MTGLE approach, the influence of the bath dynamics on the system is modeled in terms of linear harmonic chains coupled to the primary degrees of freedom, which are governed by Langevin dynamics. The authors have successfully used the

model to compute liquid and solid response functions² and to simulate inelastic gas–surface collisions, vibrational energy relaxation in solids, and radical recombination reactions in liquids.³ Berkowitz and McCammon proposed a model based on stochastic boundary conditions.⁵ They divided the many-body condensed phase system into three principal spherical regions: a reaction region, a bath region, and a static reservoir region. The motion of atoms in the reaction zone is treated with standard MD, whereas Langevin equation based stochastic dynamics is used to model the atomic motion in the bath region. The configuration of particles in the reservoir region remains fixed and provides a potential that confines the dynamics to the two inner regions. The configuration of the reservoir particles is selected from an equilibrated molecular dynamics trajectory of a larger system. Brooks and Karplus expanded this model by employing a mean field force approximation (MFFA), which computes the boundary potential based on the average influence of the particles in the reservoir region.⁶

There are several difficulties associated with this approach. As the dynamical algorithms are different for the three regions, each atom must be assigned to a particular region. When the atom crosses the boundary between the regions, the dynamical algorithm for the motion of this atom must be changed appropriately. The difficulties arise as the atoms move beyond the reservoir region during simulation. Although the MFFA was extended to simulations of aqueous systems,⁷ no provision was made to account for the polarization effects due to long-range electrostatic interactions which are dominant in polar solvents. Several attempts were made to treat the contribution of the electrostatic field to the boundary potential in an average way, including the surface constrained all atom solvent model (SCAAS) of King and Warshe^{8,9} and the reaction field with exclusion (RFE) of Rullman and van Duijnen.¹⁰

In addition, the above methods do not take into account the fluctuations of density and volume, characteristic of constant pressure conditions under which most processes of interest evolve. The latter was addressed by Beglov and Roux, who

developed the spherical solvent boundary potential (SSBP), based on the potential of mean force derived from the solvation free energy of a hard sphere containing the solute and a layer of solvent molecules nearest to the solute.¹¹ The solvation free energy is computed by a formal separation of the multidimensional solute–solvent configurational integral in terms of inner solvent molecules and the bulk solvent molecules out of the hard sphere. The hard sphere represents a configurational restriction on the outer bulk solvent molecules, and its radius fluctuates to include the most distant inner solvent molecule. The latter provides a flexible solvent boundary potential that can model volume and density fluctuations inside the sphere. The model was used to study various biomolecular systems, including the electron transfer in proteins,^{12,13} solvation^{14,15} and thermal stability of biomolecules,^{16–18} and the folding kinetics of proteins.^{19–21} The method was further generalized to non-uniform solvents through a finite difference Poisson–Boltzmann treatment of electrostatics,²² which allowed selective simulation of protein reaction centers. However the method still restricts the shape of the boundary to be either spherical or orthorhombic. Moreover, the boundary potential must be updated in every time step because it depends on the distance from the solute to the farthest inner solvent molecule. More recently, there have been several attempts to develop a more flexible boundary potential which can respond to fluctuations in the shape of the confined solute. Beglov and Roux²³ introduced the primary hydration shell method, in which a small number of solvent molecules are kept in contact with the surface of the solute through the use of a simple harmonic restraining potential, and used it to compute the relative torsional free energies of small peptide conformers. In a different approach, Lounnas, Lüdemann, and Wade introduced the shell approximation for protein hydration (SAPHYR) model,²⁴ in which a small number of explicit water molecules surrounding the solute are subject to a boundary potential consisting of a van der Waals component and an electrostatic component approximated by an average dipole–dipole interaction. The forces always act normal to the boundary surface, the position of which is dynamically adjusted based on the distance from solute atoms. The authors were able to successfully reproduce the structural properties of several solvated proteins. On the other hand, Kimura, Brower, Zhang, and Sugimori developed the surface of active polarons (SOAP) method²⁵ in which the effects of the bulk solvent are modeled by dynamically adjusting the partial charges of the oxygen atoms of explicitly represented water molecules to account for the effects of the surface charge induced on the boundary due to the polarization of the bulk solvent, while a stochastic restoring force is used to prevent their evaporation. The method was successfully used to estimate solvation free energies of ions and amino acid analogues.

In this paper, we introduce a new solvent boundary model, the fluctuating elastic boundary (FEB), that is both suitable for molecular dynamics simulations and removes some of the above restrictions. In this model, the solute and a few layers of solvent molecules are surrounded by a tight-fitting elastic bag, akin to a latex glove or a balloon, which keeps the solvent molecules close to the surface of the solute. The shape of the boundary fluctuates during the simulation and evolves dynamically to accommodate the shape fluctuations of the solute–solvent system inside. This should remove the artifacts due to the fixed shape of the boundary potential present in previous models. Hence, we expect the FEB to provide a more accurate model of solvation, with relatively few explicit solvent molecules needed to account for effects of short-range solvent–solute

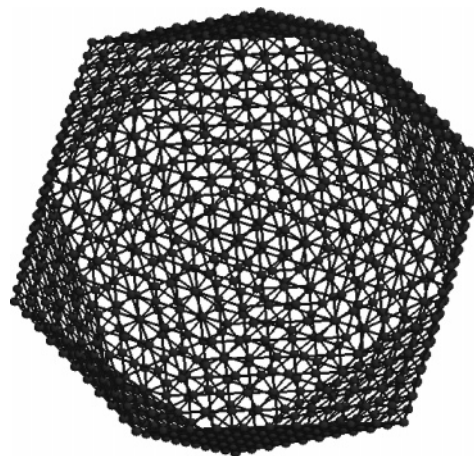


Figure 1. Fluctuating boundary bonding topology. The solid circles show the locations of the boundary quasi-particles, while the lines show the bond network. Each quasi-particle is bonded to six nearest neighbors except those on the vertexes of the icosahedron that have five bonds each.

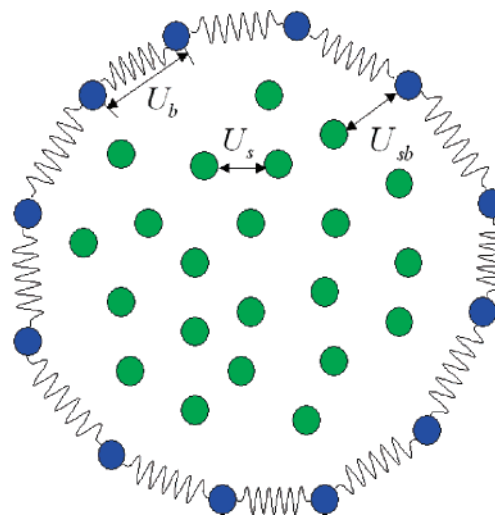


Figure 2. A diagram of the simulation cell with the FEB model. The blue circles represent the boundary quasi-particles, while the black coils indicate the elastic bonds connecting them. The green circles represent the solute–solvent system enclosed by the boundary. The principal interactions are also shown.

interactions (such as hydrogen bonding or dewetting of hydrophobic regions).

The paper is organized as follows. In section II we present the fluctuating elastic boundary model, and in section III we apply the model to the simulation of liquid argon. We conclude in section IV.

II. Method

A. Fluctuating Elastic Boundary Model. In this implementation, the elastic boundary is modeled as a network of quasi-particles, each of mass m_b , connected by elastic bonds. The resulting macromolecular arrangement has a topology of a regular icosahedron (similar to that found in fullerenes) with nearest neighbor bonds and is illustrated in Figure 1. In particular, each of the quasi-particles is bonded to 6 of its neighbors, except for the 12 particles located at the vertexes of the icosahedron. The boundary confines the solute–solvent system inside through a short-range repulsive interaction.

Figure 2 outlines the principal interactions in the solute system FEB model. The functional form of the bond potential was

chosen empirically, with the aim of providing flexibility to the boundary network, yet maintaining sufficient stiffness to prevent leakage of the solvent molecules through the boundary. In this implementation, we use a cubic interaction,

$$U_b(r_{ij}) = k_b r_{ij}^3 \quad (1)$$

where k_b is a constant governing the stiffness of the bond, and r_{ij} is the distance between two bonded boundary particles. Note that the bond potential minimum corresponds to zero bond length. Hence, in the absence of a solute–solvent system inside, all the quasi-particles would collapse to a point at zero temperature. However, at a finite temperature one would expect a nonzero average bond length even in the absence of the solute due to the thermal fluctuations of boundary particles. In addition, the cubic interaction provides a correct statistical weighing in an isobaric ensemble, which requires the boundary free energy to scale linearly with the volume. Although the latter is strictly true only for an ideal gas, nonetheless we find it to be a good starting point for further boundary potential development.

The confining potential is provided through a pairwise interaction of each of the boundary particles with the atoms of the solute–solvent system inside. The interaction form is taken to be the repulsive Lennard-Jones (LJ) of the Weeks–Chandler–Andersen (WCA) form,²⁶ given by

$$U_{sb}(r_{ij}) = \begin{cases} 4\epsilon_{sb} \left[\left(\frac{\sigma_{sb}}{r_{ij}} \right)^{12} - \left(\frac{\sigma_{sb}}{r_{ij}} \right)^6 + \frac{1}{4} \right] & r_{ij} \leq 2^{1/6} \sigma_{sb} \\ 0 & r_{ij} > 2^{1/6} \sigma_{sb} \end{cases} \quad (2)$$

where ϵ_{sb} and σ_{sb} are adjustable parameters governing the strength and the range of the boundary potential, although other choices are possible. (We have tried using the full LJ potential to model the boundary–solute interaction, but we found that this leads to increase the probability of the particle escaping the boundary. On the other hand, if the WCA potential was used these events did not occur during the course of the simulation.) This interaction models the short-range packing forces and pressure exerted by the bulk solvent on the cavity enclosed by the boundary. The repulsive potential is important to prevent the solvent molecules from escaping outside the boundary or aggregating near the boundary. Although not implemented in this study, a long-range electrostatic contribution to the boundary potential can be included through a grid-based Poisson–Boltzmann dielectric model analogous to the approach by Roux et al.²² In particular, we have recently implemented a Poisson–Boltzmann model based on the DelPhi²⁷ PB solver in the context of an MD simulation of a protein in an implicit solvent.²⁸

The adjustable parameters for this model include the mass of the boundary particles, m_b , the boundary potential parameters ϵ_{sb} and σ_{sb} , and the boundary bond constant k_b . The magnitude of the latter will determine the average pressure and hence set the density of the system at constant temperature conditions. k_b can therefore be adjusted to reproduce the ambient conditions of the solvated system. The potential parameters should be chosen according to the molecular properties of the solvent. m_b is a somewhat arbitrary parameter which determines the time scale of the boundary fluctuations and can be adjusted to allow the shape fluctuations of the boundary to evolve in parallel with the conformational dynamics of the enclosed system. In general, the choice of m_b will not influence the equilibrium configuration distribution of the solute–solvent system of interest.

B. Fluctuating Elastic Boundary Model of a Lennard-Jones Fluid. To explore the properties and validate the accuracy of the FEB model in the study of condensed phase systems, we have applied the method to the simulation of a Lennard-Jones fluid. The LJ liquid model was chosen for our initial investigation due to its computational simplicity and the availability of well-established properties from conventional simulations.²⁹

The fluctuating boundary was constructed from 1002 quasi-particles arranged in the icosahedral geometry shown in Figure 1 and connected by a network of 3000 bonds. The representative configuration of 512 LJ atoms enclosed by the boundary (subsequently referred to as the “solute”) was initially selected from a conventional molecular dynamics simulation of 1000 LJ atoms with periodic boundary conditions. The solute atoms interact with each other according to the LJ potential

$$U_s(r_{ij}) = 4\epsilon_s \left[\left(\frac{\sigma_s}{r_{ij}} \right)^{12} - \left(\frac{\sigma_s}{r_{ij}} \right)^6 \right] \quad (3)$$

where ϵ_s and σ_s are the LJ parameters governing the strength and length of the interaction, and r_{ij} is the distance between the atoms i and j . The form of the interaction potential between the solute atoms and the boundary quasi-particles is an important aspect of the model since it influences both static and dynamic properties of the solute system, especially in the regions near the boundary. In this preliminary study, we have used the WCA potential²⁶ with the LJ parameters chosen to be the same as the intersolute interactions, $\sigma_{sb} = \sigma_s$ and $\epsilon_{sb} = \epsilon_s$.

We have evaluated two simulation methods, differing in the choice of the dynamical algorithm governing the motion of boundary particles. The initial configurations of the overall boundary–solute system used in both methods were the same. A cluster of LJ atoms truncated from a larger bulk liquid system, previously equilibrated using a conventional periodic boundary condition (PBC) simulation, was placed into the regular icosahedral boundary, and the configuration of the whole system was used as the initial configuration for the FEB molecular dynamics simulation.

In the first method (which we refer to as the standard FEB model), we performed a “thermostated” simulation using the Nose–Hoover thermostats coupled to both boundary particles and solute atoms to maintain constant temperature. The value of the bond constant k_b was chosen so that the argon atoms did not escape through the boundary and the proper equilibrium density was maintained in the simulation. After the whole system reached equilibrium, we selected a number of configurations as the initial configurations for the subsequent constant energy simulations. The properties of the solute system enclosed by the boundary were calculated by averaging over the constant energy simulation trajectories.

In the second method, subsequently referred to as the thermalized FEB (TFEB) model, the Nose–Hoover thermostats were coupled only to the boundary quasi-particles, while the solute atoms were treated with standard MD. The coupling was maintained through the data collection stage as well. In this formulation, the system can exchange energy with a heat bath through interactions with the thermostated boundary, which is more in line with the canonical ensemble representation. The properties of the system were again calculated by averaging over a number of thus thermalized trajectories.

In parallel, the bulk system of 512 LJ atoms was simulated under the conventional cubic periodic boundary condition. The density of the bulk was adjusted to match that observed in the FEB model. The static and dynamic properties of the solute LJ

cluster simulated using our model were then compared with those obtained from the PBC simulations. The results are reported in the following section.

III. Simulation of Liquid Argon

We performed the FEB boundary simulation of a LJ system with the parameters consistent with the model of liquid argon ($\sigma_s = 3.41 \text{ \AA}$, $\epsilon_s = 0.2381 \text{ kcal/mol}$). A smooth cutoff was imposed on the LJ interaction at $r = 2.25\sigma_s$. For the sake of simplicity, we chose $\sigma_{sb} = \sigma_s$ and $\epsilon_{sb} = \epsilon_s$ for the parameters of the WCA potential. This is also consistent with the view of our system as comprising a cluster of argon atoms dissolved in identically interacting liquid argon solvent. We found that using larger σ_{sb} leads to the increase in the range of boundary-induced artifacts. The mass of the boundary particles was set as $m_b = 100 \text{ au}$, and the bond constant was chosen as $k_b = 0.003 \text{ kcal/(mol \AA}^3)$. These parameters allow sufficient flexibility of the boundary, while keeping the argon atoms contained throughout the simulation. All the simulations were performed using the SIM MD package³⁰ developed in our group. In both simulation methods, the system was first equilibrated through a canonical simulation at the temperature of 94.4 K. The structural and dynamic properties of the FEB model of liquid argon were computed from 10 microcanonical trajectories for the standard FEB application as well as 10 trajectories with the boundary thermalized (TFEB model). Each of the trajectories was 200 ps long generated with the time step 1 fs. The configurations were saved every 0.5 ps. The density of liquid argon in the first method was observed to be approximately $\rho = 1.42 \text{ g/cm}^3$.

A. Structural Properties. 1. Pair Correlation Function. The principal goal of the FEB method is to allow accurate simulation of localized processes in solvated systems. Hence we restricted our analysis of select properties to atoms close to the center of mass of the solvated cluster and sufficiently removed from the boundary.

We calculated the pair correlation function $g(r)$ according to

$$g(r) = \frac{1}{\rho} \frac{1}{N_c} \sum_{i|r_i < R_c} \langle \sum_{j \neq i} \delta(\mathbf{r} - \mathbf{r}_{ij}) \rangle \quad (4)$$

by considering the correlation of a subset of N_c argon atoms within a sphere radius $R_c = 5.0 \text{ \AA}$ centered at the center of mass (COM) of the argon cluster, with all the atoms in the cluster. This is in contrast with the conventional molecular dynamics simulation with periodic boundary conditions, where all atoms contribute equally to the pair correlation function. The results for $g(r)$ are shown in Figure 3. The pair correlation function obtained from the standard FEB model simulation is shown in comparison with the result obtained from a simulation using the TFEB model as well as that of bulk argon with periodic boundary conditions at the two densities $\rho = 1.42 \text{ g/cm}^3$ and $\rho = 1.405 \text{ g/cm}^3$. For $r < 12 \text{ \AA}$, both FEB model simulation results are in excellent agreement with the result obtained from the PBC molecular dynamics simulations in terms of both peak positions and heights. The first peak in both FEB models is slightly higher than the PBC counterpart, indicating a slightly higher density in the core region of the cluster. For larger distances, $g(r)$ values of both FEB models are lower than those of the PBC results. This effect is expected and is due to the finite size of our system, which leads to a drop-off of the density as we approach the boundary of the solvated cluster, with $g(r) \rightarrow 0$ as $r \rightarrow R_{\text{boundary}}$. The radial distance at which the drop-off is first observed ($r \sim 12 \text{ \AA}$) is consistent with the observed

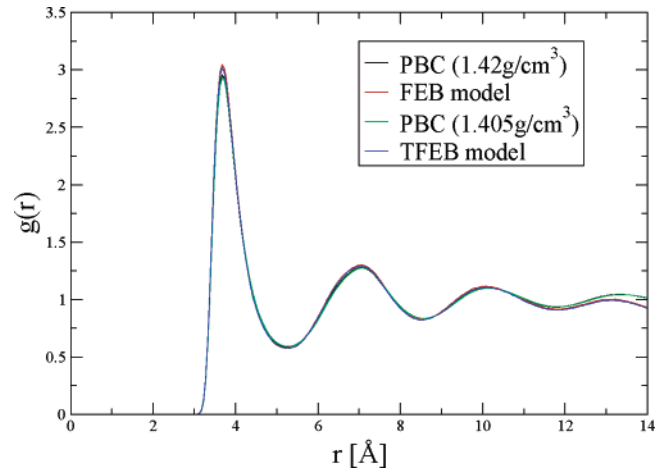


Figure 3. The pair correlation function. Black and green lines show the results of PBC simulations at densities of 1.420 g/cm^3 and $\rho = 1.405 \text{ g/cm}^3$, respectively, while the red and blue lines show the result of the standard FEB model and TFEB model simulations, respectively. Both models show excellent agreement for the first three peaks with the PBC results.

TABLE 1: Kinetic Energy and Potential Energy (in kcal/mol) of the Argon Atoms in the Two FEB Models and Two Conventional PBC Simulations^a

	kinetic energy	potential energy
FEB model	0.280	-2.690
TFEB model	0.281	-2.684
PBC model ($\rho = 1.420 \text{ g/cm}^3$)	0.285	-2.656
PBC model ($\rho = 1.405 \text{ g/cm}^3$)	0.280	-2.640

^a The values for the standard FEB and the TFEB models were computed for the particles in the core region, and the agreement with PBC results is excellent.

average radius of gyration of the boundary ($R_g \sim 21 \text{ \AA}$) and the range of the repulsive solute–boundary interaction.

2. Kinetic and Potential Energy. We compared the average per-particle kinetic and potential energy of argon atoms in the two FEB models to those computed from a molecular dynamics simulation using PBC in Table 1. The potential energy was computed according to

$$\langle U \rangle = \left\langle \frac{1}{N_c} \sum_{i|r_i < R_c} U_s(r_{ij}) \right\rangle \quad (5)$$

by averaging all pair-interactions of N_c atoms contained in the sphere of radius $R_c = 5.0 \text{ \AA}$ centered at the COM of the solute cluster, and all solute atoms within the range of interaction. In the above equation, $r_{ij} = |\mathbf{r}_i - \mathbf{r}_j|$ and U_s is given by eq 3 for $r_{ij} < r_c$ where $r_c = 2.25\sigma_s$. The values of the average per-particle potential energy are close to each other for the two models. The potential energy is slightly lower which is consistent with the higher core density for the FEB models observed from the pair correlation data.

The kinetic energy was likewise computed for the atoms in this core region according to

$$\langle T \rangle = \left\langle \frac{1}{N_c} \sum_{i|r_i < R_c} \frac{1}{2} m v^2 \right\rangle \quad (6)$$

The average per-particle kinetic energy obtained from FEB models is a little lower than that in the conventional simulation due to a slight difference in effective temperatures, which was the consequence of the removal of COM motion for the whole

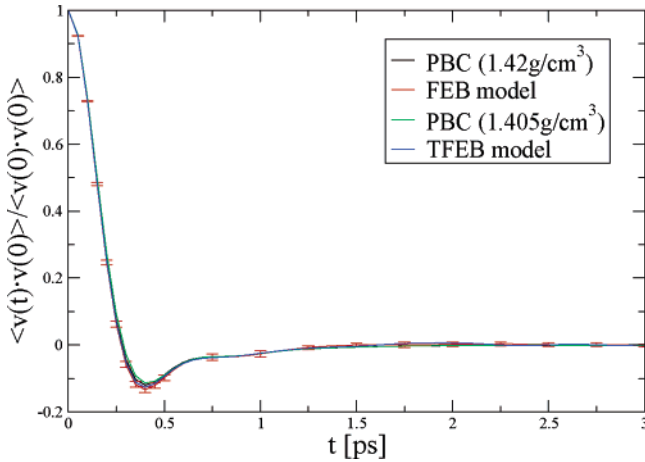


Figure 4. The velocity autocorrelation function. Black and green lines show the results of conventional simulation with periodic boundary conditions at densities of 1.420 g/cm^3 and $\rho = 1.405 \text{ g/cm}^3$, respectively. The red line shows the result of the standard FEB model simulation, and the blue line is the result of the TFEB model simulation. Representative error bars are shown for the standard FEB model (red line). Both models show excellent agreement over the entire correlation time.

system in the FEB method. Overall, both kinetic and potential energy are in excellent agreement with the PBC result.

B. Dynamic Properties. 1. *Velocity Autocorrelation Function.* The normalized velocity autocorrelation function

$$C_{vv}(t) = \frac{1}{\langle v^2 \rangle} \langle \mathbf{v}(0) \cdot \mathbf{v}(t) \rangle \quad (7)$$

gives a sensitive characterization of the dynamics of the system and provides the means for computing the self-diffusion coefficient via the Green–Kubo relation in eq 9. The velocity autocorrelation function is computed according to

$$C_{vv}(t) = \frac{1}{N_c \langle v^2 \rangle} \sum_{i|r_i(0) < R_c} \langle \mathbf{v}_i(0) \cdot \mathbf{v}_i(t) \rangle \quad (8)$$

with only the trajectories initiating in the core region ($r_i(0) < R_c = 5.0 \text{ \AA}$) contributing to the ensemble average. Figure 4 shows the velocity autocorrelation functions for the two PBC molecular dynamics simulations and the two FEB models. The results for both FEB models show very good agreement with that of the PBC molecular dynamics simulations and for the most part are within the standard error of each other. Particularly good agreement is observed between the TFEB model and the higher density PBC simulation result. The minimum of the C_{vv} of the FEB model is slightly deeper than that of the PBC result, while their positions are very close. This is also consistent with the higher core density of the FEB model cluster. The long time tails of the C_{vv} computed via the two FEB models are well behaved with a smooth decay to zero in ~ 5 ps and fluctuations that are small compared with the PBC results. This allows the self-diffusion coefficient to be computed from the velocity autocorrelation data using the Green–Kubo relation,

$$D = \frac{1}{3} \int_0^\infty \langle \mathbf{v}(0) \cdot \mathbf{v}(t) \rangle \quad (9)$$

The integrals were evaluated numerically for all four functions up to $t = 5$ ps, and the results are shown in Table 2. The diffusion coefficient computed from the FEB model is slightly

TABLE 2: Diffusion Coefficients (in $\text{\AA}^2/\text{ps}$), Computed from the Mean Square Displacement (MSD) and the Velocity Autocorrelation Function (VAC)^a

	MSD	VAC
PBC model ($\rho = 1.420 \text{ g/cm}^3$)	0.193	0.193
PBC model ($\rho = 1.405 \text{ g/cm}^3$)	0.200	0.200
FEB model	0.195 ± 0.019	0.191 ± 0.015
TFEB model	0.209 ± 0.026	0.195 ± 0.016

^a The results are shown for the PBC simulations at two different densities as well as the standard FEB and the TFEB simulations. The one standard deviation error bars (also in $\text{\AA}^2/\text{ps}$) are computed by block averaging.

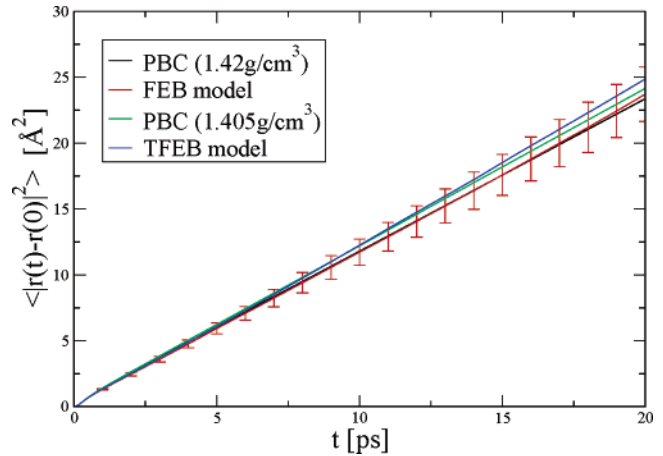


Figure 5. The mean square displacement function. The black line shows the result of a PBC model simulation at density of $\rho = 1.420 \text{ g/cm}^3$, and the green line shows the PBC simulation result at $\rho = 1.405 \text{ g/cm}^3$. The red line shows the result of the standard FEB model simulation, and the blue line gives the result of the TFEB model. Representative error bars are shown in red for the FEB model. The agreement is good over the entire range of 20 ps.

lower than that obtained using PBC, due to a somewhat higher cluster core density, but the overall agreement is very good.

2. *Mean Square Displacement.* The mean square displacement function,

$$\langle \Delta R^2(t) \rangle = \langle |\mathbf{r}(t) - \mathbf{r}(0)|^2 \rangle \quad (10)$$

provides another characterization of the dynamics of the system and allows the calculation of the self-diffusion coefficient via the Einstein relation,

$$D = \frac{1}{6} \lim_{t \rightarrow \infty} \frac{d}{dt} \langle \Delta R^2(t) \rangle \quad (11)$$

The results for the two FEB models were computed as in the previous section, by counting only those trajectories which originated in the core region, $r(0) < R_c$ (and hence far away from the boundary), according to

$$\langle \Delta R^2(t) \rangle = \frac{1}{N_c} \sum_{i|r_i(0) < R_c} \langle |\mathbf{r}_i(t) - \mathbf{r}_i(0)|^2 \rangle \quad (12)$$

Figure 5 displays the mean square displacement (MSD) functions computed from the two FEB models and the two PBC simulations of liquid argon. It is apparent from the plot that the FEB model results exhibit a partial nonlinear behavior. This is due to the drift motion of the COM of the argon cluster that is induced by the low frequency modulations in the shape of the elastic boundary. The effect is somewhat more severe in the TFEB model as it was not possible to remove the total COM

motion, since the latter is not conserved. Nevertheless, it is possible to extract the diffusion coefficient through linear regression fits. The values of the latter obtained for FEB and PBC simulations in this fashion are shown in Table 2. Although the diffusion coefficients are in good agreement, the nonlinear nature of the mean square displacement curve for the FEB model does introduce ambiguity in the Einstein relation approach for computing diffusion coefficients. Moreover, since the liquid is confined, the MSD will eventually level off as it approaches the values of the square of the average boundary radius. In addition, the large uncertainty, particularly at long times, that is evident from the size of the error bars, makes it difficult to estimate the accuracy of our model vis-à-vis the PBC results.

The methods for computing the transport coefficients based on the Kubo-like transport functions, such as the velocity or displacement autocorrelation function based techniques described above, in general apply only to infinite, bulk fluids. Although it is possible, using these techniques, to extract information on diffusion in a confined system, such as our bag, great care should be taken to ensure one considers only the length and time scales on which the effect of the confinement on the bulklike properties is minimal.³¹ In our case, this implies computing time correlation functions for the atoms that are located near the center of the bag, and far away from the edges, and do not stray far from this region throughout the analysis time. This restriction results in a small fraction of generated particle trajectories being suitable for diffusion analysis, thus limiting the statistical quality of the results. To overcome this limitation, an alternate, more suitable approach is presented in the following section.

3. Diffusion Operator Eigenfunction Autocorrelation Functions. In the previous section, we have demonstrated how self-diffusion coefficients in bulk liquids can be accurately computed from the displacement correlation function via the Einstein relation. We have also shown how the diffusion coefficient can be computed from the velocity autocorrelation function via the Green–Kubo relation. The latter method is generally less stable numerically as it requires accurate determination of the long time tails of the velocity correlation function. However both of these methods assume a uniform distribution at infinite time, which is generally not the case for a system enclosed by the elastic boundary. Such a system exhibits a pronounced density deficit in the region near the boundary. Hence the above methods would be applicable only in regions far away from the boundary and not very suitable for computing the diffusion coefficient in this system. An alternate method was recently proposed³¹ for determining diffusion coefficients of fluids in confined regions and near interfaces. We present a modified approach in this study.

In a homogeneous bulk fluid, we can model the self-diffusion by “labeling” certain particles, without changing their properties in any way. The conditional distribution of these labeled particles $K_s(\mathbf{r}, t|\mathbf{r}_0, 0)$, which is the probability of finding a particle at \mathbf{r} at time t given it was at \mathbf{r}_0 initially, would then obey the classic diffusion equation:

$$\frac{\partial}{\partial t} K_s(\mathbf{r}, t|\mathbf{r}_0, 0) = D\nabla^2 K_s(\mathbf{r}, t|\mathbf{r}_0, 0) \quad (13)$$

To estimate the diffusion in a finite region of space, we define a virtual boundary surface \mathcal{S}_b as a sphere of radius R_b , centered at the COM of the fluid. The boundary is considered to be absorbing, so that $K_s(\mathbf{r} \in \mathcal{S}_b, t) = 0$. The family of functions

that satisfy eq 13 and these boundary conditions are given by

$$\Psi_{klm}(\mathbf{r}, \theta, \phi) = j_l(kr)Y_l^m(\theta, \phi) \quad (14)$$

where j_l are the spherical Bessel functions and Y_l^m are the spherical harmonics. The absorbing boundary condition requires that $k_l R_b$ be equal to the roots of j_l and leads to the orthogonality of the eigenfunctions,

$$\langle \Psi_{klm} | \Psi_{k'l'm'} \rangle = \frac{1}{2} R_b^3 |j_{l+1}(kR_b)|^2 \delta_{ll'} \delta_{mm'} \delta_{kk'} \quad (15)$$

The above functions form a complete orthonormal set. Any conditional probability distribution satisfying eq 13 can then be written in terms of this set of eigenfunctions,

$$K_s(\mathbf{r}, t|\mathbf{r}_0, 0) = \sum_{klm} \Psi_{klm}(\mathbf{r}_0) \Psi_{klm}^*(\mathbf{r}) e^{-k^2 D t} \quad (16)$$

A family of diffusion operator eigenfunction autocorrelation functions can then be defined as

$$C_{klm}(t) = \langle \Psi_{klm}(\mathbf{r}(t)) \Psi_{klm}(\mathbf{r}(0)) \rangle = \int d\mathbf{r} \int d\mathbf{r}_0 p_s(\mathbf{r}, t; \mathbf{r}_0, 0) \Psi_{klm}(\mathbf{r}) \Psi_{klm}(\mathbf{r}_0) \quad (17)$$

where $p_s(\mathbf{r}, t; \mathbf{r}_0, 0)$ is the joint probability distribution, defined as the probability of finding a particle at \mathbf{r} at time t and a particle at \mathbf{r}_0 initially. The joint probability distribution can be expressed in terms of the conditional probability distribution as

$$p_s(\mathbf{r}, t|\mathbf{r}_0, 0) = K_s(\mathbf{r}, t|\mathbf{r}_0, 0) p_s(\mathbf{r}_0, 0) \quad (18)$$

where $p_s(\mathbf{r}_0, 0)$ is the initial distribution. Equation 17 can then be written as

$$C_{klm}(t) = \langle \Psi_{klm}(\mathbf{r}(t)) \Psi_{klm}(\mathbf{r}(0)) \rangle = \int d\mathbf{r} \int d\mathbf{r}_0 K_s(\mathbf{r}, t|\mathbf{r}_0, 0) p_s(\mathbf{r}_0, 0) \Psi_{klm}(\mathbf{r}) \Psi_{klm}(\mathbf{r}_0) \quad (19)$$

Taking the initial distribution to be uniform, $p_s(\mathbf{r}_0, 0) = \bar{p}_{s0}$ (which is appropriate for a bulk solvent), and using the orthogonality property of eq 15, it can be shown that

$$C_{klm}(t) = e^{-k^2 D t} \int d\mathbf{r}_0 |\Psi_{klm}(\mathbf{r}_0)|^2 \bar{p}_{s0} \quad (20)$$

Hence, $C_{klm}(t) \propto \exp[-k^2 D t]$ and the diffusion coefficient can be obtained from $C_{klm}(t)$ by

$$D = -\frac{1}{k_l^2} \frac{d}{dt} \ln[C_{klm}(t)] \quad (21)$$

Note that in theory any $C_{klm}(t)$ can be used in computing the diffusion coefficient, but only at sufficiently long times to allow for all initial effects to decay. This means one should use only the smallest eigenvalues of the diffusion operator. In practice, one should select the eigenfunctions for which $C_{klm}(t)$ exhibits appreciable, but not too fast, decay over the time scale accessible by simulation, and which are not too oscillatory as the latter slows down convergence. In this work, we use the four low order eigenfunctions, with klm equal to 100, 110, 200, and 211.

The above results are derived based on the assumption that the self-diffusion in a liquid system is adequately described by eq 13. On the other hand, a confined system such as a fluid enclosed by the fluctuating boundary would exhibit a non-

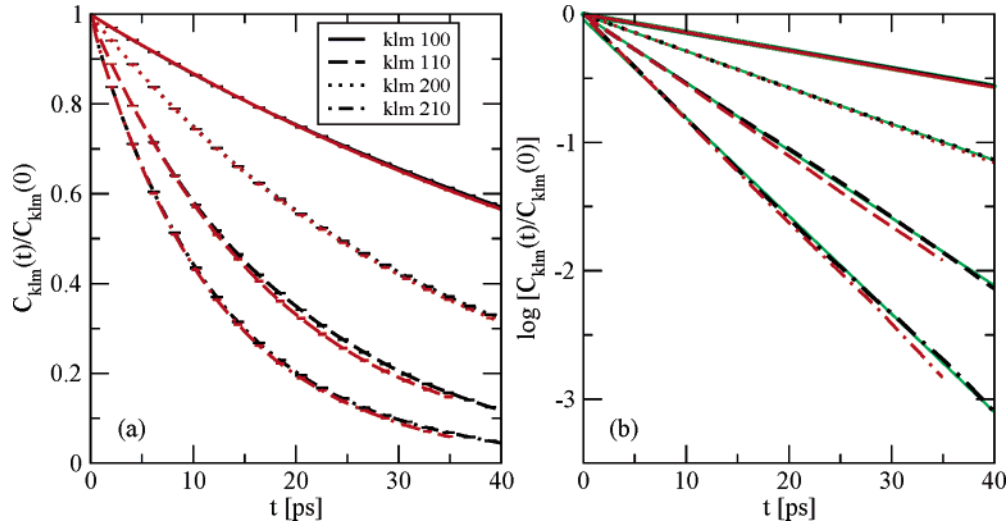


Figure 6. Diffusion eigenfunction autocorrelation functions (a) and their respective logarithms (b) are shown for the several low lying members of the family. Black lines correspond to the standard FEB model results, while the red lines show the results obtained from the TFEB model. The green lines show linear regression fits to the standard FEB model in panel b. All the functions are well-behaved and show good exponential decay with correct decay constants.

TABLE 3: Self-Diffusion Coefficients in $\text{\AA}^2/\text{ps}$ for Liquid Argon Enclosed by the Fluctuating Boundary, Extracted from Four Low Order Diffusion Eigenfunction Autocorrelation Functions, with the Corresponding Eigenvalues k_l^a

function	k_l	FEB	TFEB
$C_{100}(t)$	0.2617	0.204 ± 0.010	0.209 ± 0.013
$C_{200}(t)$	0.5236	0.194 ± 0.012	0.213 ± 0.033
$C_{110}(t)$	0.3744	0.204 ± 0.016	0.207 ± 0.012
$C_{210}(t)$	0.6438	0.190 ± 0.016	0.208 ± 0.029

^a The data are shown for the FEB model and the TFEB model with one standard deviation error bars computed by block averaging.

uniform equilibrium distribution and hence is better described by the Smoluchowski equation:

$$\nabla \cdot \mathbf{D} \cdot [\nabla + \beta(\nabla W(\mathbf{r}))] K_s(\mathbf{r}, t | \mathbf{r}_0, 0) = \frac{\partial}{\partial t} K_s(\mathbf{r}, t | \mathbf{r}_0, 0) \quad (22)$$

where $W(\mathbf{r})$ is the potential of mean force derived from the equilibrium distribution. A complete discussion of these points is available in ref 31. Nonetheless, we expect our treatment to give accurate results, since our absorbing boundary is located sufficiently far from the FEB and the radius of this ‘‘virtual cavity’’ is large compared to corrections to the boundary position observed in the previous studies.

Figure 6a shows four low order eigenfunction correlations (ECF) for the argon system, computed by placing a virtual boundary at $R_b = 12.0 \text{ \AA}$ from the COM of the argon droplet. The ECF were computed for both the standard FEB model (black lines) as well as the thermalized (TFEB) simulation (red lines). All cases exhibit a decay tail that is exponential to high degree of accuracy. A least-squares fit to the $\ln[C(t)]$ shown as green lines in Figure 6b was used to extract the diffusion coefficients for both models, which are shown, along with accompanying eigenvalues k_l , in Table 3. All are in good agreement with the results of PBC simulations of bulk argon and within standard error of each other. In particular, the lower order slower decaying eigenfunctions C_{100} and C_{200} fit exponential decays more closely than their faster counterparts and exhibit tighter error bars. This is not surprising as nondiffusive ballistic motion plays a more prominent role at shorter time scales which dominate the latter. In addition, higher order Bessel

functions are more oscillatory which leads to increased statistical uncertainty evident from larger error bars.

4. Boundary Shape Fluctuation Dynamics. Finally, we investigated the dynamics of the shape fluctuations of the elastic boundary. The understanding of the latter is important in designing a boundary that would successfully adapt to conformational changes of the solute system, while preserving the solvation properties and not introducing too many dynamic artifacts. In particular, we examine the radial dynamics of the boundary, which is the only degree of freedom in the Beglov–Roux SSBP model.^{11,22} This motion can be described via a dynamic radius of gyration of the boundary quasi-particles,

$$R_g(t) = \sqrt{\frac{\sum_j m_b |\mathbf{r}_j(t) - \mathbf{r}_{CM}(t)|^2}{\sum_j m_b}} \quad (23)$$

where j runs over all boundary particles, and r_{CM} is their center of mass. Figure 7a shows $R_g(t)$ computed for three randomly chosen microcanonical trajectories of the standard FEB liquid argon model. The radial fluctuations are very small, on the order of 0.2 \AA , indicating a stable, equilibrium system. The oscillations are quasi-periodic with an estimated period of $\sim 25 \text{ ps}$, which is much slower than the time scale of motion of the argon atoms inside. We next examined the anisotropic fluctuations of the boundary by computing the inertia tensor anisotropy autocorrelation function (ICF) $C_{\Delta I}$, defined as the dyadic colon product of the anisotropic inertia tensor residuals,

$$C_{\Delta I} = \langle \Delta \mathbf{I}(0) : \Delta \mathbf{I}(t) \rangle = \left\langle \sum_{ij} \Delta I_{ij}(0) \Delta I_{ji}(t) \right\rangle \quad (24)$$

with

$$\Delta \mathbf{I} = \mathbf{I} - \text{Tr}(\mathbf{I}) \mathbf{1} \quad (25)$$

where \mathbf{I} is the inertia tensor of the boundary quasi-particle system and $\mathbf{1}$ is the unit tensor. The ICF provides insight into the nature and the time scale of the deviations of boundary shape from a perfectly isotropic spherical object. Hence it complements the gyration radius, which provides an estimate of volume

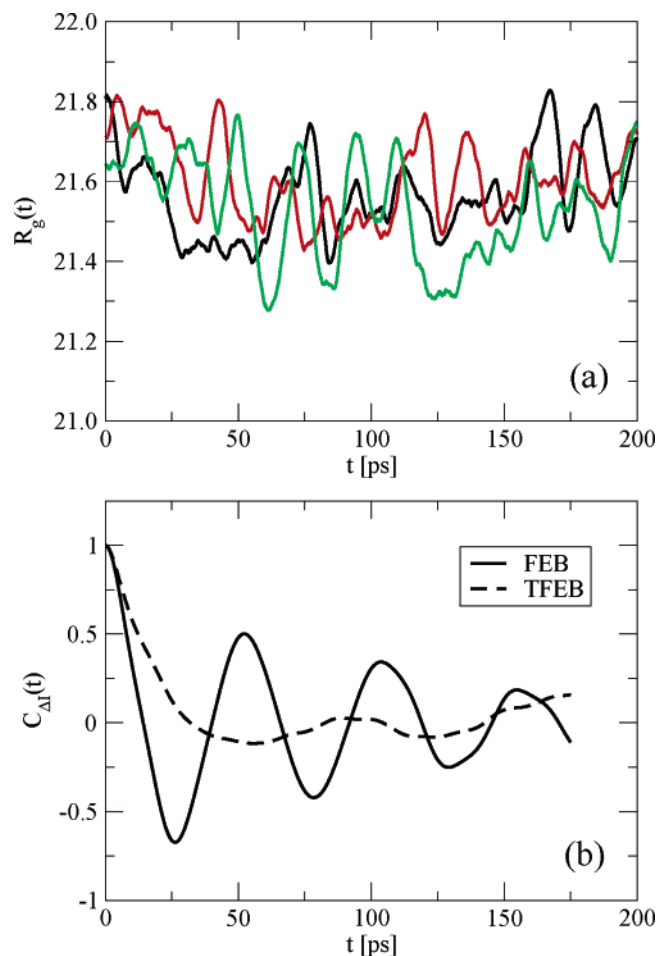


Figure 7. Boundary fluctuation dynamics. The radius of gyration of the boundary as a function of time is shown in panel a for three randomly selected microcanonical trajectories (black, red, and green). The inertia tensor anisotropy autocorrelation function is shown in panel b for the first method (all-constant energy) (solid) and the second method (thermostated boundary) (dashed).

fluctuation of the bounded cavity, with the information on fluctuations of the shape. In Figure 7b, we show the normalized ICF for the standard FEB with the argon cluster as the solid line. The correlation data show pronounced periodicity, with slow dephasing and coherence that persists over more than 200 ps. Moreover, the coherent fluctuations are dominated by low frequency modes, with an average period of ~ 50 ps, or about twice the period of radial fluctuations. Given that the correlations in the argon dynamics dissipate much more rapidly (on the order of ~ 5 ps, as evident from the velocity correlation function data), we do not expect significant dynamic coupling between these boundary modes and the argon cluster. For comparison, we also show the result obtained from the TFEB simulation (dotted line). In this case the decoherence occurs much more rapidly, as the boundary particles are able to dissipate energy much more effectively through coupling with the thermostats than in the constant energy simulation. In the latter the only channel through which dissipation was possible was weak coupling to the argon cluster. Hence, we would expect the TFEB model to provide a more uniform representation of the fluctuating boundary and reduce the occurrence of boundary-induced artifacts that affect the dynamics of the enclosed system.

IV. Conclusions

A fluctuating elastic boundary model has been introduced for circumventing the difficulties associated with the conven-

tional periodic boundary condition. We studied a cluster of liquid argon using this new approach. Both structural and dynamic properties calculated from the FEB models in two different implementations are in excellent agreement with the results of the conventional molecular dynamics simulation.

In this paper, we considered an atomic solvent surrounded by an elastic boundary, but the concept of the FEB model can be applied to simulations of more general systems. In particular, a long-range electrostatic contribution to the boundary potential can be incorporated through the use of a Poisson–Boltzmann model by representing the region outside the boundary as a dielectric continuum. This would allow the model to be applied to charged systems, such as polar solvents (primarily water) as well as solvated biomolecules. We expect that the FEB and TFEB models will be valuable tools in the study of the dynamics of biomolecules. For example, this would include the simulation of the dynamics of the protein and surrounding solvent in the protein-folding process. The shape of the boundary would vary conforming to the configuration change of the protein. This should allow proper simulation of solvation using just a few explicit solvent molecules to simulate the bulk solvent.

Acknowledgment. This work was supported by a grant to B.J.B. from the National Science Foundation (CHE-03-16896). We acknowledge Byungchan Kim and Edward Harder for useful discussions regarding the implementation of the TFEB model and developing the diffusion eigenfunction method.

References and Notes

- (1) Allen, M. P.; Tildesley, D. J. *Computer Simulation of Liquids*; Oxford University Press: Oxford, 1987.
- (2) Berkowitz, M.; Brooks, C. L., III; Adelman, S. A. *J. Chem. Phys.* **1980**, *72*, 3889.
- (3) Brooks, C. L., III; Berkowitz, M.; Adelman, S. A. *J. Chem. Phys.* **1980**, *73*, 4353.
- (4) Adelman, S. A.; Brooks, C. L., III. *J. Phys. Chem.* **1982**, *86*, 1511.
- (5) Berkowitz, M.; McCammon, J. A. *Chem. Phys. Lett.* **1982**, *90*, 215.
- (6) Brooks, C. L., III; Karplus, M. *J. Chem. Phys.* **1983**, *79*, 6312.
- (7) Brunger, A.; Brooks, C. L., III; Karplus, M. *Chem. Phys. Lett.* **1984**, *105*, 495.
- (8) Warshel, A.; King, G. *Chem. Phys. Lett.* **1985**, *121*, 124.
- (9) King, G.; Warshel, A. *J. Chem. Phys.* **1989**, *91*, 3647.
- (10) Rullman, J. A.; van Duijnen, P. T. *Mol. Phys.* **1987**, *61*, 293.
- (11) Beglov, D.; Roux, B. *J. Chem. Phys.* **1994**, *100*, 9050.
- (12) Basu, G.; Kitao, A.; Kuki, A.; Go, N. *J. Phys. Chem. B* **1998**, *102*, 2076.
- (13) Basu, G.; Kitao, A.; Kuki, A.; Go, N. *J. Phys. Chem. B* **1998**, *102*, 2085.
- (14) Roux, B. *Biophys. J.* **1996**, *71*, 2076.
- (15) Nina, M.; Beglov, D.; Roux, B. *J. Phys. Chem. B* **1997**, *101*, 5239.
- (16) Sugita, Y.; Kitao, A. *Proteins* **1988**, *30*, 388.
- (17) Sugita, Y.; Kitao, A. *Biophys. J.* **1988**, *75*, 2178.
- (18) Sugita, Y.; Kitao, A.; Go, N. *Folding Des.* **1988**, *27*, 173.
- (19) Marchand, S.; Roux, B. *Proteins* **1988**, *33*, 265.
- (20) Mohanty, D.; Elber, R.; Thirumalai, D.; Beglov, D.; Roux, B. *J. Mol. Biol.* **1997**, *272*, 423.
- (21) Kitao, A.; Hayward, S.; Go, N. *Proteins* **1988**, *33*, 496.
- (22) Im, W.; Bernèche, S.; Roux, B. *J. Chem. Phys.* **2001**, *114*, 2924.
- (23) Beglov, D.; Roux, B. *Biopolymers* **1995**, *35*, 171.
- (24) Lounnas, V.; Lüdemann, S. K.; Wade, R. C. *Biophys. Chem.* **1999**, *78*, 157.
- (25) Kimura, S. R.; Brower, R. C.; Zhang, C.; Sugimori, M. *J. Chem. Phys.* **2000**, *112*, 7723.
- (26) Chandler, D.; Weeks, J. D.; Andersen, H. C. *Science* **1983**, *220*, 787.
- (27) Honig, B.; Nicholls, A. *Science* **1995**, *268*, 1144.
- (28) Zhou, R.; Krilov, G.; Berne, B. J. *J. Phys. Chem. B* **2004**, *108*, 7528.
- (29) Rahman, A. *Phys. Rev. A* **1964**, *136*, A405.
- (30) Stern, H.; Xu, H.; Harder, E.; Ritter, F.; Pavese, M.; Berne, B. J. Unpublished, 2000.
- (31) Liu, P.; Harder, E.; Berne, B. J. *J. Phys. Chem. B* **2004**, *108*, 6595.